American Mineralogist, Volume 73, pages 956–965, 1988

Calculation of equilibrium crystallization paths of compositionally simple hydrous felsic melts

HANNA NEKVASIL*
Geology Department, Arizona State University, Tempe, Arizona 85287, U.S.A.

ABSTRACT

A method has been developed for calculating crystallization paths and generating phase-assemblage diagrams for compositions in the "granite" system (i.e., the system Ab-An-Or-Qz-H_2O). The phase-assemblage diagrams for a synthetic adamellite and tonalite at 2- and 8-kbar total pressure were calculated to permit comparison with available experimental data. The agreement is favorable at 2 kbar with greater discrepancies at 8 kbar, particularly for the plagioclase-saturation curves. The method was also applied to the calculation of H_2O-buffered crystallization paths in order to delineate differences between crystallization paths of melts under H_2O-undersaturated, unbuffered conditions and those of melts under the buffering influence of a H_2O-CO_2 fluid. A method is presented that permits the determination of variations in H_2O content of the melt and of remaining liquid during crystallization without modal analysis.

INTRODUCTION

Phase relations in the model granite system Ab-Or-An-Qz-H_2O and their variations with H_2O content and total pressure provide invaluable information regarding phase relations of natural felsic melts. In order to supplement the limited available experimental data on phase relations in the granite system, Nekvasil and Burnham (1987) used the revised quasi-crystalline model (Burnham and Nekvasil, 1986) to predict quantitatively both H_2O-saturated and H_2O-undersaturated liquidus phase relations in the bounding subsystems of the "granite"-H_2O system. Although such information is vital to the evaluation of liquidus relations of felsic melts, it is very difficult to determine, quantitatively, the crystallization paths from geometric constraints of the five-component system. If the phase relations in the "granite" system are to be used to interpret the crystallization history of natural and synthetic felsic melts, a calculation scheme must be developed that yields the temperature of appearance of each crystalline phase as well as the abundances and compositions of all phases in the temperature interval between the liquidus and solidus.

As the simplest case, it is important to understand the nature of equilibrium crystallization paths. The closed-system constraint of equilibrium crystallization permits the use of relatively simple mass-balance relations. Once closed-system equilibrium paths can be precisely defined, departures from closed-system behavior can be more readily detected and evaluated. Inasmuch as felsic melts so commonly show evidence of disequilibrium (e.g., zoned feldspars), equilibrium crystallization is not a likely process, particularly during the late stages of crystallization. A step-wise fractional crystallization process may more reasonably model the crystallization behavior. Step-wise fractional crystallization can be modeled as a simple variation of equilibrium crystallization by removing, at a chosen increment of temperature or crystal abundance, the crystals that have precipitated during the fractionation increment.

CALCULATION METHODOLOGY

The calculation methodology used can be subdivided into thermodynamic compositional relations and mass-balance relations. For a given melt composition, total pressure (P) and temperature (T), the thermodynamic compositional relations determine which crystalline phases are present (i.e., with which phases the melt is saturated) and the compositions of these phases. The mass-balance relations enforce the closed nature of the system and require that the total abundances of all components remain constant.

The thermodynamic compositional relations used in the calculations of crystallization paths are those used to calculate crystal/melt equilibria in hydrous melts in the "granite" system (Nekvasil and Burnham, 1987). If a melt containing component i coexists stably with a crystalline phase containing i, the chemical potentials of i in solid and melt can be equated to yield the following expression

$$\ln(a_i^m/a_i^s) = -(\Delta G_i^{0,m}(1,T) + \int \Delta V_i^m dP)/RT, \quad (1)$$

where a_i^m and a_i^s refer to the activities of i in the melt and solid phases, respectively, and $\Delta G_i^{0,m}$ and ΔV_i^m refer to the standard-state free energy of fusion and volume of fusion of i, respectively. The $\Delta G_i^{0,m}$ for the components Ab, An, Or, and Qz (Si_4O_8) refer to the pure components in crys-

* Present address: Department of Earth and Space Sciences, State University of New York at Stony Brook, Stony Brook, New York 11794-2100, U.S.A.

0003–004X/88/0910–0956$02.00

talline and melt phases at 1 atm and T such that the $a_i = 1$.

From Equation 1 above, the saturation temperature of Si_4O_8 can be readily determined using the expressions for the activity-composition relations of Qz in the melt as a function of melt composition, pressure, and H_2O content and the expression for $\Delta G^{0,m}_{Qz}$ (both presented in Burnham and Nekvasil, 1986). For the feldspar components, however, an additional complexity arises from their solution in the two feldspars, plagioclase and alkali feldspar. If the ternary nature of these solid solutions is taken into account, the constraint that $\Sigma X_i = 1$ yields the following expression

$$(a^m_{Ab}/\gamma^{Pl(Af)}_{Ab})\exp[(\Delta G^{0,m}_{Ab}(1,T) + \int \Delta V\, dP)/RT] +$$
$$(a^m_{Or}/\gamma^{Pl(Af)}_{Or})\exp[(\Delta G^{0,m}_{Or}(1,T) + \int \Delta V\, dP)/RT] +$$
$$(a^m_{An}/\gamma^{Pl(Af)}_{An})\exp[(\Delta G^{0,m}_{An}(1,T) + \int \Delta V\, dP)/RT] = 1.0, \quad (2)$$

where a^m_i refers to the activity of i in the anhydrous or hydrous melt and γ_i to the activity coefficient of i in either plagioclase or alkali feldspar. Expressions for the activity-composition relations of the feldspar components in melts lying within the granite tetrahedron have been presented in Burnham and Nekvasil (1986) and can be used to evaluate the activities of component i in the anhydrous melt (a^{am}_i). To convert to activities in the hydrous melt (a^{hm}_i), the albite-H_2O model (Burnham, 1975) was used. This conversion uses the expressions

$$a^{hm}_i = a^{am}_i(1 - X_w)^2 \quad (3a)$$

for X_w (mole fraction of H_2O) ≤ 0.5 and

$$a^{hm}_i = 0.25a^{am}_i\exp\{(6.52 - 2667/T)[\ln(1 - X_w) + X_w + 0.193]\} \quad (3b)$$

for $X_w > 0.5$.

In order to calculate feldspar-melt equilibria, the activity-composition relations of Nekvasil and Burnham (1987) for the feldspar components in ternary solid solution were used. Table 1 gives the interaction parameters for the three components Ab, An, and Or. The expressions for the activities of these components (modified from Ghiorso, 1984) are in Appendix 1. These expressions differ from those of Ghiorso (1984) because the interaction parameters obtained by Nekvasil and Burnham (1987) from the data of Seil and Blencoe (1979 and pers. comm.) for binary plagioclase (instead of the H^{ex} of Newton et al., 1980) obviated use of the Al-avoidance entropy model. Instead, the entropy of mixing in the ternary solid solution was expressed on the basis of the three end-member components, resulting in the following expression for the free energy of mixing

$$G^{mix} = G^{ex} - T[-R(X_{Ab}\ln X_{Ab} + X_{An}\ln X_{An} + X_{Or}\ln X_{Or})]. \quad (4)$$

Figure 1 shows the calculated ternary-feldspar solvus at the temperatures and pressures of Seck's (1971a, 1971b) data. The solvus was calculated using the activity-matching algorithm described by Barron (1976). At 650 °C and 1 kbar (Fig. 1a), the experimental data differ from the calculated compositions to the greatest extent; the calculated plagioclase compositions are higher in Or content (by a few wt%) than the experimental compositions. At 900 °C and 0.5 kbar (Fig. 1c), the solubility of Or in anorthitic plagioclases is underestimated by a few mol%. These differences, although significant if suitability for geothermometry is being considered, have little effect on compositional variation during differentiation of felsic melts. This conclusion was reached by comparison of phase-assemblage diagrams calculated on the basis of ternary-feldspar–melt equilibria and binary-feldspar–melt equilibria. Equilibrium temperatures for the two-feldspar pairs listed by Ghiorso (1984) but based on the equations in Appendix 1 and parameters of Table 1 have been compared with those obtained by Ghiorso (1984) and Fuhrman and Lindsley (1988). The comparisons indicate the same extent of variability between the computed equilibrium temperatures and experimental temperatures as observed by these workers. Calculation of phase relations for subsystems in the "granite" system using the activity-composition relations for the ternary feldspars of Nekvasil and Burnham (1987) and those for the melt components from Nekvasil (1986) (as listed in Burnham and Nekvasil, 1986) have already been conducted and comparisons with available experimental data have been discussed in Nekvasil and Burnham (1987).

Mass-balance relations can be readily obtained from consideration of the stages that a crystallizing system must pass through as the temperature drops to the solidus. As a completely molten magma cools, the chemical potentials (μ_i) of all components in both crystalline and melt phases increase. However, owing to the larger partial molar entropy ($\bar{S}_i$) for the components in the melt phase relative to the $\bar{S}_i$ for those in solids, the change in μ_i per unit change in temperature (T) will be greater for the components in the melt phase. At some temperature, the μ_i vs. T curves for the components in the solid phase and those for the corresponding components in the melt phase will cross (i.e., $\mu^m_i = \mu^s_i$) and the temperature of intersection will mark the onset of the precipitation of the liquidus phase from the melt (i.e., at this temperature, the melt has become saturated with crystalline phase 1). At

TABLE 1. Interaction parameters for the feldspars

Interacting components			Coefficients	
a_1	a_2	Parameter	a	b
Ab	Or*	a_1, a_2	7404	−5.120
		a_2, a_1	4078	—
Ab	An	a_1, a_2	3377	−1.476
		a_2, a_1	2683	−1.882
An	Or	a_1, a_2	5980	2.581
		a_2, a_1	17931	−5.494

Note: W_{a_1,a_2} $W_{a_2,a_1} = a + bT$ (T in kelvins, W in calories) for the asymmetric, binary, regular-solution formulation $G^{ex}_{a_1,a_2} = W_{a_1,a_2}X_{a_1}X^2_{a_2} + W_{a_2,a_1}X^2_{a_1}X_{a_2} + W_vPX_{a_1}X_{a_2}$, where $W_{v(Or,Ab)} = 0.086$ cal/bar; P in bars (Thompson and Hovis, 1979).

* From Thompson and Hovis (1979).

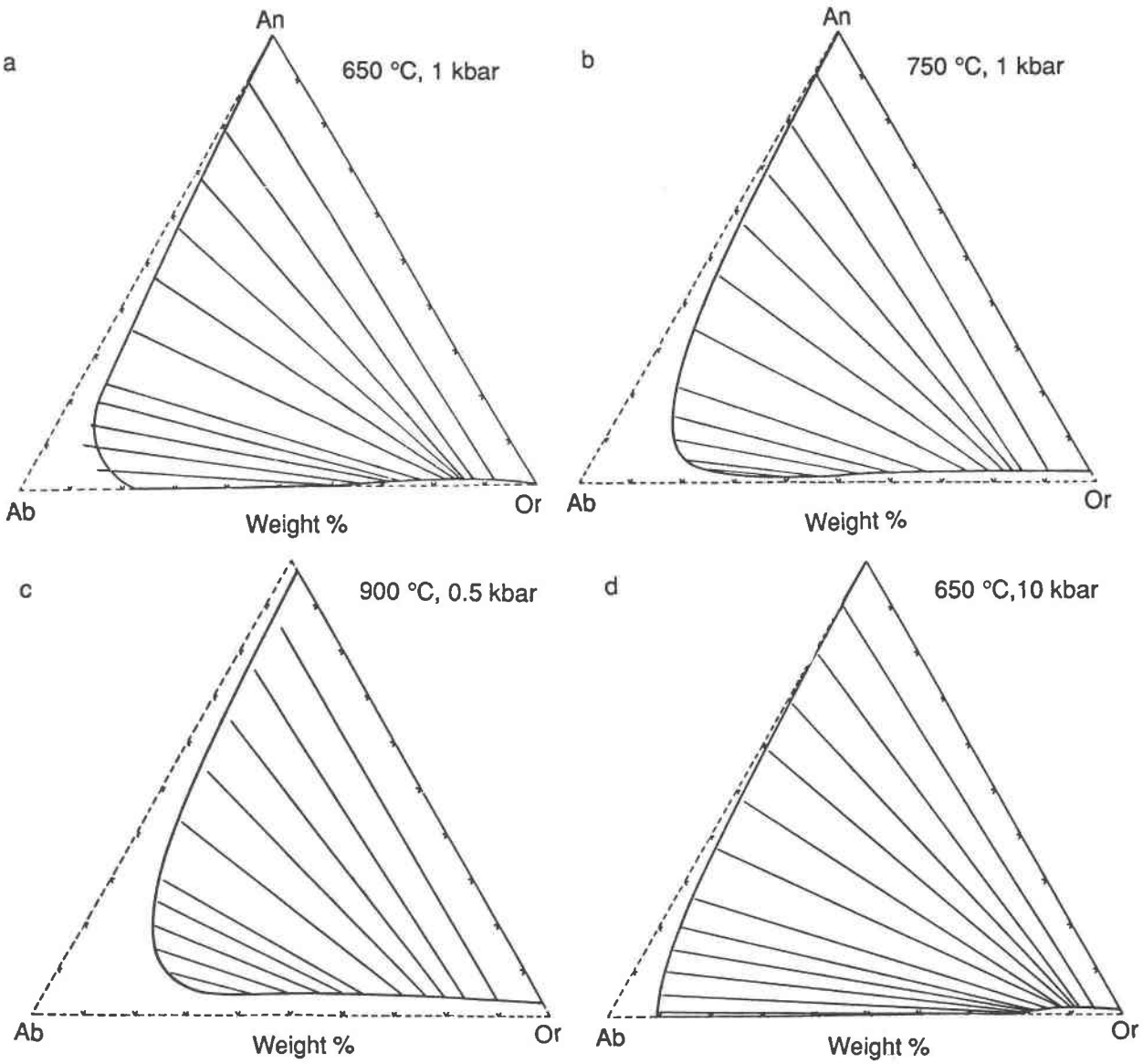

Fig. 1. Calculated isothermal, isobaric solvus cross sections (solid curves) based upon the mixing parameters in Table 1 and expressions of App. 1. The tie lines are based on the data of Seck (1971a, 1971b).

any temperature, the proportions of melt, solid, and fluid phases (X_L, X_S, X_V, respectively) are constrained to sum to 1. Therefore, as the temperature continues to drop, the fraction of liquid [F_L ($=X_L$)] will decrease, the amount of crystals (X_S) will increase, and the melt will be continuously depleted in the component(s) (e.g., i) included in the solid phase and enriched in the excluded components (e.g., j) (because $X_i^{hm} + \Sigma X_j^{hm} = 1$). The new melt composition at T' is dependent upon the amount and composition of the crystalline phase precipitated; however, the amount and composition of the phase precipitated depends on the new melt composition. This interdependence of variables necessitates the use of an iterative process to satisfy the conditions that (1) the basic equation of equilibrium (Eq. 1) holds for all components in the crystalline phase, (2) the excluded melt components increase in concentration to $X_j^{hm} = X_j^{hm^0}/F_L$ (where $X_j^{hm^0}$ refers to the mole fraction of component j in the initial hydrous melt), (3) $\Sigma X_j^{hm} + X_i^{hm} = 1$ (and, if phase 1 is a solid solution, the mole fractions of its components must also sum to 1), and (4) F_L is described by the following expression (if one crystalline phase coexists with melt):

$$F_L^{hm} = [X_i^{hm^0} - X_i^{s1}(1 - X_v)]/(X_i^{hm} - X_i^{s1}),$$

where X_i^{s1} is the mole fraction of component i in crystalline phase 1 and X_v the mole fraction of exsolved H_2O vapor in the system (which is 0 if the system is H_2O-undersaturated at T''). X_v is described by the relation

$$X_v = X_w^0 - F_L[X_{w,sat}^m],$$

where $X_{w,sat}^m$ is the saturation mole fraction of H_2O.

As the melt continues to cool, the chemical potentials and activities of the excluded melt components rise not only due to their dependence on T, but also because of their increased concentration. Eventually, at T'', phase 2 (S_2) begins to precipitate. At least one feldspar must be crystallizing when S_2 begins to coprecipitate with S_1. The changing melt composition, crystal composition, and phase proportions must now be computed iteratively using the equations of equilibrium for at least three components. If quartz represents one of the two crystalline phases, then only H_2O will increase in the melt by $1/F_L$, otherwise, both H_2O and Qz will increase in this manner. If the system is H_2O-saturated however, H_2O content will increase only as a result of temperature and compositional dependence of the activity of H_2O.

Two additional equations are needed to obtain all of the information about the system at T''. These can be obtained by evaluating F_L twice, with two different sets of components. (The resulting expressions for F_L and X_{S_1} and X_{S_2} are in App. 2.) Once the phase compositions and proportions are obtained at T'', Equations 1 and 2 are used to determine whether the melt has become saturated with the last crystalline phase. Additionally, $X_{w,sat}^m$ is calculated and compared with X_w to determine whether the melt has become saturated with respect to an aqueous fluid. Once three crystalline phases are present (providing that the bulk composition is sufficiently Or and An rich), the calculation methodology is modified for use of the appropriate expression for F_L (see App. 2), and the solidus is determined as that temperature at which $F_L = 0$).

This calculation scheme can be extended to any number of crystalline phases coexisting with a melt through the following general expression (derived in App. 2) for F_L (fraction of hydrous melt in the system):

$$F_L^{hm} = [X_i^{hm^0} - X_i^{S_1}(1 - X_{S_2} - X_{S_3} - X_{S_4} - \cdots - X_v) - X_i^{S_2}(1 - X_{S_1} - X_{S_3} - X_{S_4} - \cdots - X_v) - X_i^{S_3}(1 - X_{S_1} - X_{S_2} - X_{S_4} - \cdots - X_v) - \cdots]/(X_i^{hm} - X_i^{S_1} - X_i^{S_2} - X_i^{S_3} - \cdots).$$

Expressions for X_{S_1}, X_{S_2}, etc., can be obtained by using several components and manipulating the resulting expressions. For the calculation (Nekvasil-Coraor and Burnham, 1983, 1984), A FORTRAN 77 routine has been developed that uses the bulk melt composition, the total pressure, and the initial H_2O content of the melt as input variables. The liquidus temperature and phase composition are calculated first. Then, for various temperatures below the liquidus, phase compositions and proportions are calculated until the melt becomes saturated with the second phase. The saturation temperature of the second phase and the phase compositions and proportions at this temperature are computed. Similar calculations yield the phase assemblages as crystallization continues to the temperature of appearance of the third phase as well as the temperature at which H_2O saturation is achieved. At small temperature increments below the temperature of onset of precipitation of the third phase, the phase assemblages are monitored until $F_L = 0$ within the tolerance of the iterations.

Comparison of calculated and experimentally determined phase-assemblage diagrams

Phase-assemblage diagrams in which temperature is plotted against the H_2O content of the system (i.e., initial H_2O content of the melt) indicate the effect of H_2O content on the saturation temperatures of the crystalline phases. Several characteristics of the crystalline-phase saturation curves can be predicted from the thermodynamic properties of the components in the "granite" system. The squared relationship of X_w to a_w in Equation 3a implies that the extent of lowering of the saturation temperatures with increasing H_2O content per unit change in X_w should diminish as X_w increases. The much smaller $\Delta H_{Qz}^{0,m}$ relative to the feldspar components implies that the saturation temperatures of quartz will change to a greater extent per increment increase in X_w (see discussion in Nekvasil and Burnham, 1987) unless the melt component mixing behavior were grossly nonideal. Therefore, the slope of the quartz saturation curve will be much steeper than for the feldspars (as seen in Fig. 2). This characteristic implies that compositions for which the saturation temperature of quartz is only slightly higher than that for either one of the feldspars at low bulk H_2O content will likely have a change in the sequence of appearance of these phases at high bulk H_2O contents. This "cross-over" phenomenon is an important indicator of bulk H_2O content.

Unbuffered phase-assemblage diagrams often indicate the positions of "H_2O solubility" curves and the H_2O-saturated solidi. Caution must be exercised when interpreting the nature of such "H_2O solubility" curves, however. These curves indicate the solubility of H_2O in the initial melt only at their intersection with the saturation curve for the liquidus phase. At temperatures below the liquidus they indicate, for a specific bulk H_2O content of the system, at what temperature (and, less directly, at what fraction of liquid remaining) the melt (with unspecified H_2O content) will become saturated with H_2O. The "H_2O saturation" curves do not indicate the H_2O content of the melt upon the attainment of H_2O saturation below the liquidus temperature. It is readily apparent that, although useful in predicting phase assemblages, such diagrams yield no direct information regarding the changes in melt and crystalline phase proportions or compositions (including H_2O content) during crystallization.

The calculated phase-assemblage diagrams for a synthetic adamellite and tonalite at 2- and 8-kbar total pressure are given in Figure 2. The compositions of the adamellite and tonalite are in Table 2 and are those used by

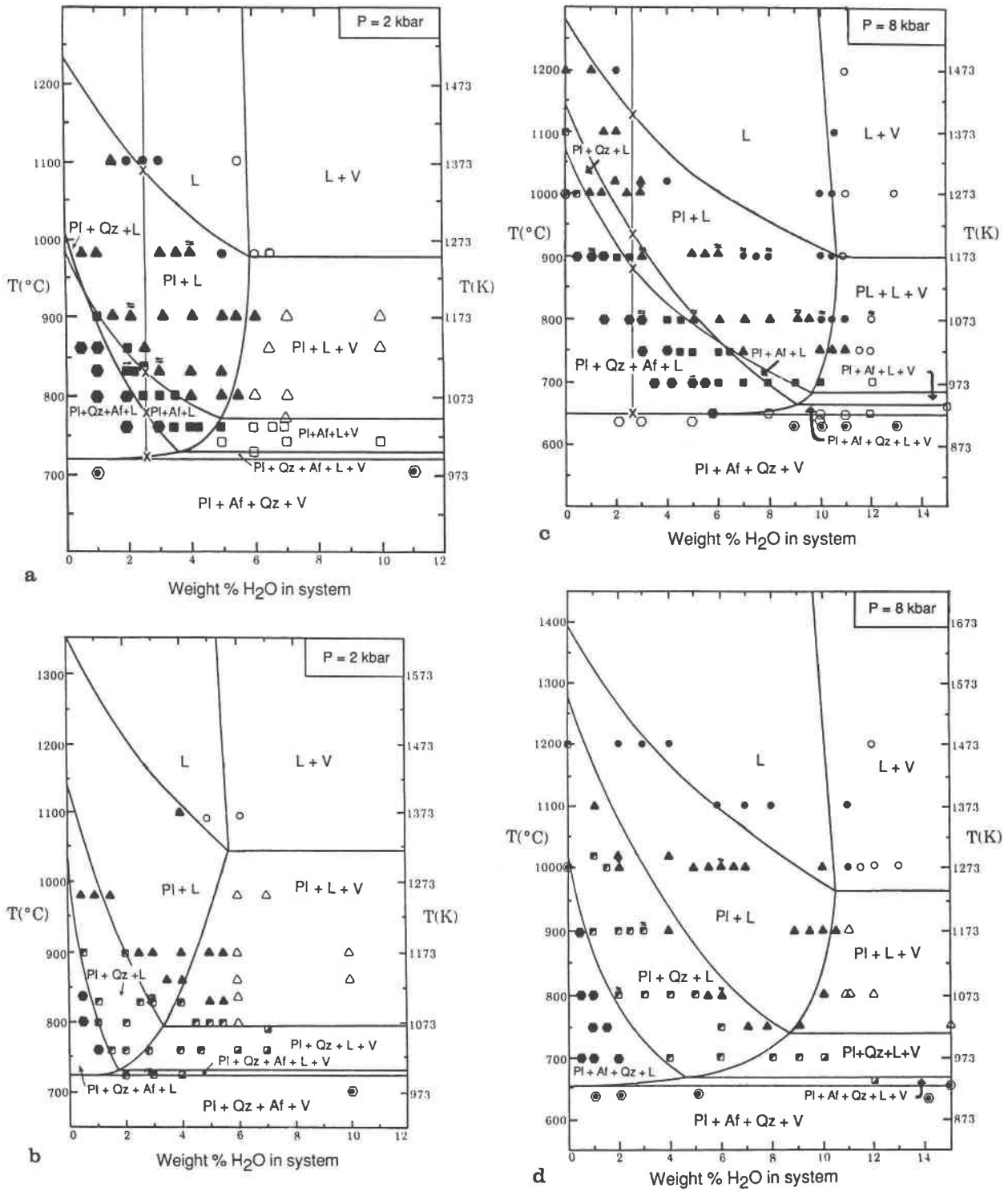

Fig. 2. Calculated H_2O-unbuffered phase-assemblage diagrams for the synthetic adamellite and tonalite at 2-kbar (**a** and **b**, respectively) and at 8-kbar total pressure (**c** and **d**, respectively). The experimental data of Whitney (1975) are also plotted to facilitate comparison. Symbols are defined in the above symbol key. The unbuffered crystallization paths for the adamellite and tonalite compositions with 2.8 wt% H_2O are denoted by the vertical lines. The × symbols along this line indicate the saturation temperatures of the crystalline phases.

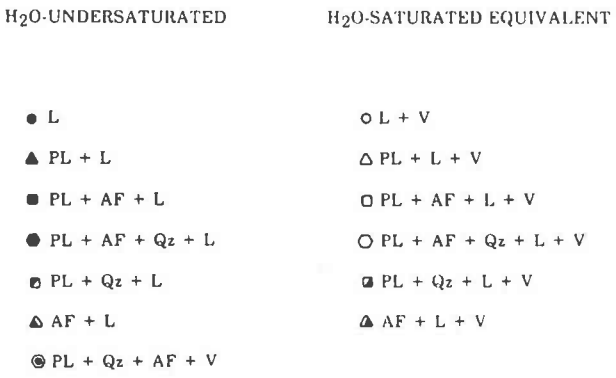

Fig. 2—*Continued.*

Whitney (1975) in his experimental investigation of the phase-assemblage relations. The calculated crystalline-phase saturation curves at 2 kbar generally agree with the data of Whitney (1975), the differences being greatest for the plagioclase saturation surface. The 8-kbar results agree less well, the discrepancy being greatest once again for the plagioclase saturation curve for the adamellite. There is, however, an internal inconsistency among the experimental data. For the adamellite, the data indicate a zero to slightly negative P-T slope for plagioclase (for a given H_2O content in the H_2O-undersaturated region) unlike for the other crystalline phases. For the tonalite, however, the P-T slope of the plagioclase saturation curve is positive. It is difficult to envision how such a small difference in bulk composition and even smaller differences between the plagioclase compositions along the liquidus could result in such radically different characteristics. The differences between the 8-kbar calculated curves and experimental data for the other crystalline phases are minor. These discrepancies could arise if the activity-composition relations between the feldspar (An in particular) and Qz melt components were significantly in error. The discrepancies, however, could also be a result of experimental uncertainty at high pressure due to the lower equilibration temperatures induced by higher H_2O solubilities (see Nekvasil and Burnham, 1987). Nonetheless, the overall agreement permits the use of the predicted relations to obtain crystallization trends in the system.

Comparison of the calculated "H_2O saturation" curves with the data of Whitney (1975) in Figure 2 indicates that there is a recurring discrepancy between the calculated and experimental results in the position of the calculated "H_2O saturation curve." It is this curve, however, that is likely to be the most difficult to determine experimentally because it indicates the incipient exsolution of an aqueous phase. It is likely that some finite amount of undercooling would occur during the nucleation of vapor bubbles, which would have to be magnified to permit them to be visible optically. That the discrepancy is always in the direction of the calculated solubility curve lying at higher temperatures (or lower H_2O contents) may indicate such a phenomenon. Furthermore, the "H_2O solubility" curves determined by Whitney (1975) for the adamellite and tonalite at 2 kbar indicate internal inconsistencies. There is little difference between the position of these curves in these two diagrams. Yet, the more silica-rich and Or-poor nature of the latter composition and the large temperature interval over which plagioclase crystallizes alone and enriches the melt in silica should result in H_2O saturation at an earlier stage of the crystallization temperature interval because of the lower solubility of H_2O in silica melts relative to feldspar melts (Kennedy et al., 1962). A more reasonable configuration may well be represented by the curves in Figures 2b and 2d.

TABLE 2. Synthetic compositions used in the crystallization-path calculations

Molecular constitutent*	Compositional type	
	Adamellite	Tonalite
Qz	0.236	0.295
Ab	0.344	0.318
Or	0.286	0.105
An	0.134	0.282

* Eight-oxygen molecular norm.

H_2O-BUFFERED VS. UNBUFFERED CRYSTALLIZATION PATHS

In order to circumvent the problems inherent in phase-equilibrium experiments on H_2O-undersaturated felsic melts in the absence of a fluid phase, some recent experimentation has been conducted under H_2O-undersaturated but vapor-present conditions through the use of H_2O-CO_2 fluids for which the H_2O content of the fluid is less than 100 mol% (e.g., Clemens and Wall, 1981; Clemens et al., 1986; Webster et al., 1987). These experiments are conducted under the premise that, if sufficiently large volumes of fluid (H_2O-CO_2 mixture) are in contact with a melt, the H_2O content of the melt will be buffered by the fluid, and exsolution of H_2O from the melt during crystallization will not significantly affect the H_2O:CO_2 ratio of the fluid. The phase-assemblage relations obtained in this manner yield the saturation temperatures of the crystalline phases and the solidus for an essentially constant a_w of the melt. Once again, the melt compositions and phase proportions will change as crystallization proceeds, but the H_2O content will change only in response to the dependence of a_w on melt composition and temperature. Figures 3a and 3b show the calculated phase-assemblage diagram for the synthetic adamellite at 2 and 8 kbar, respectively, for H_2O-buffered conditions. The differences between H_2O-unbuffered and buffered crystallization paths are readily manifested in the differences between the saturation temperatures (cf. Figs. 2 and 3). The crystalline-phase saturation temperatures are higher for the buffered case than the unbuffered case for all except the liquidus phase. Inasmuch as a great portion of crystallization in natural systems is likely to occur under unbuffered conditions, it is apparent that the simple use of H_2O-buffered phase-assemblage diagrams to determine the saturation temperatures and sequence of appearance of the crystalline phases will lead to erroneous results. If,

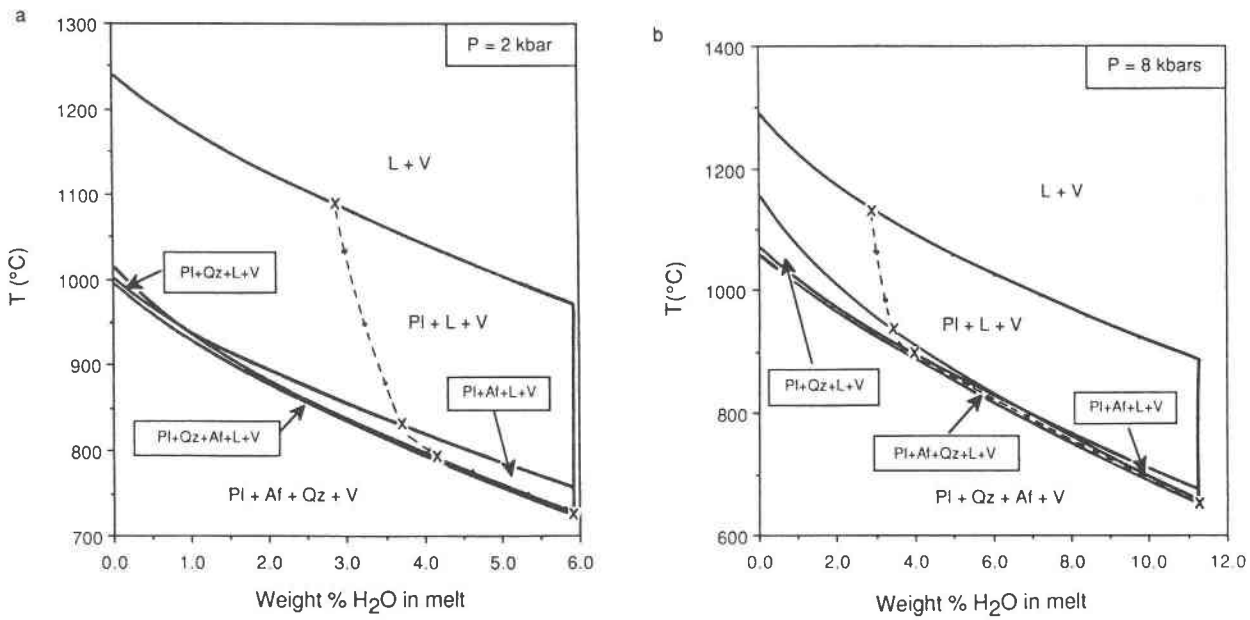

Fig. 3. Calculated H_2O-buffered phase-assemblage diagrams for the synthetic adamellite at (a) 2-kbar and (b) 8-kbar total pressure. The dashed curves indicate the unbuffered crystallization paths for 2.8 wt% H_2O as shown in Figs. 2a, and 2c.

however, the variation in H_2O content during crystallization of an initially H_2O-undersaturated melt were known, the buffered phase-assemblage diagram becomes useful in the interpretation of crystallization histories. Analytical determinations of the variation in H_2O content of a crystallizing melt is difficult but may become more feasible in future investigations as techniques using the ion microprobe and infrared spectroscopy are perfected and become more accessible. A more indirect method of obtaining this variation would be to obtain good approximations of the modal variation with temperature, but this is a tedious process potentially fraught with error.

There is, however, an alternative method to determine the variation in H_2O content during crystallization from experimental investigation that obviates the need for direct H_2O or modal abundance analysis. The calculated unbuffered crystallization paths for 2.8 wt% H_2O in the system at 2- and 8-kbar total pressure of Figures 2a and 2c are shown plotted onto the H_2O-buffered phase-assemblage diagrams by the dashed curves in Figures 3a and 3b. The crosses indicate the crystalline-phase saturation temperatures of Figures 2a and 2c. At each intersection of the unbuffered crystallization paths with the H_2O-buffered crystalline-phase saturation curves, the composition of the melt, crystalline phases, phase proportions, and H_2O content are the same for both unbuffered and buffered conditions. This relationship indicates that if saturation temperatures are determined for an unbuffered composition at a bulk H_2O content of interest and the phase-assemblage diagram for the buffered case is also determined at this and higher H_2O contents, then plotting the unbuffered crystalline-phase saturation temperatures on the buffered diagram will yield a locus of points describing the variation in H_2O content of the melt. Additionally, since the H_2O content in the melt is increasing as X_w^0/F_L until hydrous phases are stabilized, the variation in fraction of melt remaining can also be obtained from the locus described by the saturation temperatures.

The trend in variation of H_2O content and thus fraction of hydrous melt (F_L) with temperature shown in Figures 3a and 3b is characteristic of H_2O-unbuffered crystallization paths. If the initial H_2O content were high, H_2O saturation would be achieved at a temperature much above the solidus. As crystallization continued, the H_2O content of the melt would no longer increase as X_w^0/F_L (as would be the case under H_2O-saturated conditions) but rather would remain relatively constant. This variant on the path would also be expected if a hydrous mineral began to crystallize whose presence buffered the H_2O content of the melt during further crystallization.

Figures 4a and 4b show the calculated variation in phase proportions of the synthetic adamellite with 2.8 wt% initial H_2O content of the melt during unbuffered crystallization at 2- and 8-kbar total pressure, respectively. At temperatures very close to the solidus, there is a marked increase in the extent of crystallization with temperature, that is, a large amount of crystallization occurs along the five-phase curve (Af + Pl + L + Qz + V) during a very small (several degrees) change in temperature. Investigation of the phase relations of the "granite" tetrahedron and, in particular, the nature of this limiting curve (Nekvasil and Burnham, 1987; Nekvasil, 1988) indicates that the temperature change *along* this curve is slight; hence, crystallization along it proceeds with marked changes in composition induced by very small changes in

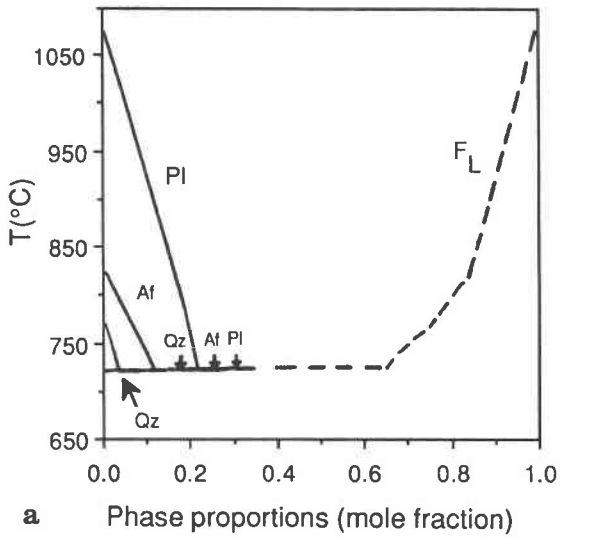

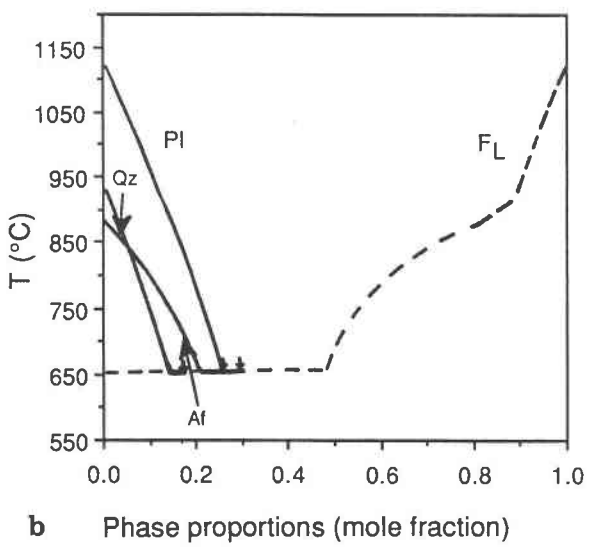

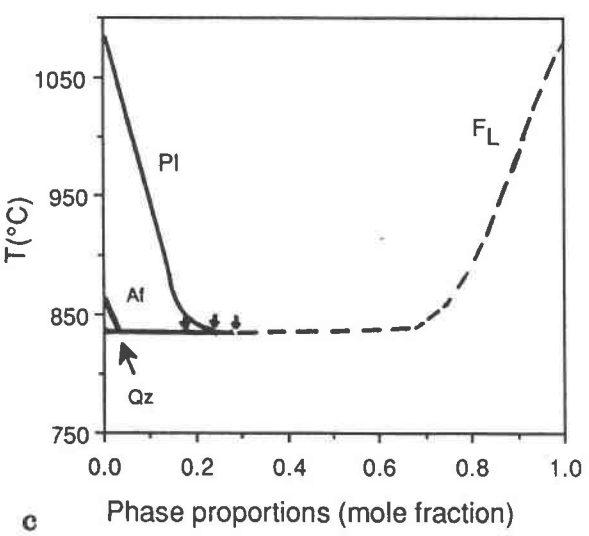

←

Fig. 4. Calculated variation in proportions of melt (F_L), plagioclase (X_{pl}), quartz (as Si_4O_8, X_{qz}), and alkali feldspar (X_{af}) during H_2O-unbuffered crystallization of the synthetic adamellite with 2.8 wt% H_2O in the system at (**a**) 2-kbar and (**b**) 8-kbar total pressure. The calculated variation in phase proportions during H_2O-buffered crystallization at 2 kbar for the adamellite with 2.8 wt% H_2O in the melt is shown in (**c**) for comparison. All phase proportions are given in mole fraction of the system such that $F_L + X_{pl} + X_{qz} + X_{af} + X_v$ (exsolved H_2O) = 1. The small arrows indicate the final (i.e., solidus) proportions of the crystalline phases (as labeled in 4a).

temperature. The marked change in the calculated variations in phase abundances with temperature near the solidus as seen in Figures 4a and 4b is thus a reflection of the melt reaching the H_2O-saturated five-phase curve.

If the marked decrease in fraction of liquid remaining in the system with slight temperature decrease is a result of the melt reaching and sliding along the H_2O-saturated five-phase curve in the "granite" system, then this effect should also be noticeable for crystallization proceeding under buffered conditions as the melt slides along a four-phase (or five-phase) H_2O isoactivity curve. In this case, however, the marked change in F_L should begin precisely when the third phase begins to precipitate, that is, when the melt reaches a four-phase (or five-phase) H_2O isoactivity curve. Such behavior is shown in Figure 4c, which shows the variation in phase proportions during crystallization under H_2O-buffered conditions for the adamellite with 2.8 wt% H_2O in the melt.

In conclusion, it was the intent of this article to indicate how the revised quasi-crystalline model (Burnham, 1981; Burnham and Nekvasil, 1986) can be used to calculate crystallization paths. Comparison of the calculated paths with experimental data indicates reasonable agreement at low pressure but greater deviations at high pressures. The crystallization-path calculation methodology permits the prediction of H_2O-buffered as well as H_2O-unbuffered phase-assemblage relations. The calculations, however, also provide valuable information on how the phase proportions and compositions change during crystallization. Through such calculations, it can be shown that the relationship between the two types of diagrams can be used to obtain information regarding the changing phase proportions simply from experimental investigation of crystalline-phase saturation temperatures. Although the calculations certainly yield more complete information than is reasonably extracted from phase-stability experiments, the calculations are currently restricted to compositions lying in the "granite" system. The understanding of phase relations of more compositionally complex granitoids must come from further careful experimentation.

Acknowledgments

This work was supported in part by the National Science Foundation grants EAR 82-12492 awarded to C. Wayne Burnham and EAR 86-17128 awarded to J. R. Holloway, which are gratefully acknowledged. The helpful reviews of J. Longhi, R. Luth, J. Holloway, and C. Wayne Burnham

were greatly appreciated and resulted in numerous improvements to the manuscript.

References cited

Barron, L.M. (1976) A comparison of two models of ternary excess free energy. Contributions to Mineralogy and Petrology, 57, 71–81.

Burnham, C.Wayne. (1967) Hydrothermal fluids at the magmatic stage. In H.L. Barnes, Ed., Geochemistry of hydrothermal ore deposits (lst edition), p. 34–76. Holt, Rinehart and Winston, New York.

——— (1975) Thermodynamics of melting in experimental silicate-volatile systems. Geochimica et Cosmochimica Acta, 39, 1077–1084.

——— (1981) Nature of multicomponent aluminosilicate melts. In D.T. Rickard and F.E. Wickman, Eds., Chemistry and geochemistry of solutions at high temperatures and pressures. Physics and chemistry of the Earth, 13–14, 197–229.

Burnham, C. Wayne, and Nekvasil, H. (1986) Equilibrium properties of granite pegmatite magmas. American Mineralogist, 71, 239–263.

Clemens, J.C., and Wall, V.J. (1981) Origin and crystallization of some peraluminous (S-type) granitic magmas. Canadian Mineralogist, 19, 111–131.

Clemens, J.C., Holloway, J.R., and White, A.J.R. (1986) Origin of an A-type granite. American Mineralogist, 71, 317–324.

Fuhrman, M.L., and Lindsley, D.H. (1988) Ternary-feldspar modeling and thermometry. American Mineralogist, 73, 201–215.

Ghiorso, M.S. (1984) Activity-composition relations in ternary feldspars. Contributions to Mineralogy and Petrology, 87, 282–296.

Kennedy, G.C., Wasserburg, G.J., Heard, H.C., and Newton, R.C. (1962) The upper three-phase curve in the system SiO_2-H_2O. American Journal of Science, 260, 501–521.

Nekvasil, H. (1986) A theoretical thermodynamic investigation of the system Ab-Or-An-Qz(-H_2O) with implications for melt speciation. Ph.D. thesis, The Pennsylvania State University, University Park.

——— (1988) Calculated effect of anorthite component on the crystallization paths of H_2O-undersaturated haplogranitic melts. American Mineralogist, 73, 966–981.

Nekvasil, H., and Burnham, C.W. (1987) The calculated individual effects of pressure and water content on phase equilibria in the granite system. In B.O. Mysen, Ed., Magmatic processes: Physicochemical principles. Geochemical Society Special Publication 1, 433–445.

Nekvasil-Coraor, H., and Burnham, C.Wayne. (1983) Thermodynamic modelling of crystallization paths of felsic melts. Geological Society of America Abstracts with Programs, 15, 651.

——— (1984) Thermodynamic modelling of crystallization paths of felsic melts: The haplogranite and haplogranodiorite systems. Geological Society of America Abstracts with Programs, 16, 609.

Newton, R.L., Charlu, T.V., and Kleppa, O.J. (1980) Thermochemistry of high structural state plagioclases. Geochimica et Cosmochimica Acta, 44, 933–941.

Seck, H.A. (1971a) Koexistierende Alkalifeldspate und Plagioklase im System $NaAlSi_3O_8$-$CaAl_2Si_2O_8$-$KAlSi_3O_8$-H_2O bei Temperaturen von 650°C–900°C. Neues Jahrbuch für Mineralogie Abhandlungen, 115, 315–345.

——— (1971b) Der Einfluss des Druckes auf die Zusammensetzung koexistierende Alkalifeldspate und Plagioklase im System $NaAlSi_3O_8$-$CaAl_2Si_2O_8$-$KAlSi_3O_8$-H_2O. Contributions to Mineralogy and Petrology, 31, 67–86.

Seil, M.K., and Blencoe, J.G. (1979) Activity-composition relations in $NaAlSi_3O_8$-$CaAl_2Si_2O_8$ feldspars at 2 kbar, 600–800°C. Geological Society of America Abstracts with Programs 11, 513.

Thompson, J.B., and Hovis, G.L. (1979) Entropy of mixing in sanidine. American Mineralogist, 64, 57–65.

Webster, J.D., Holloway, J.H., and Hervig, R.L. (1987) Phase equilibria of a Be-, U- and F-enriched vitrophyre from Spor Mountain, Utah. Geochimica et Cosmochimica Acta, 51, 389–402.

Whitney, J.A. (1975) The effect of pressure, temperature, and $X(H_2O)$ on phase assemblages in four synthetic rock compositions. Journal of Geology, 83, 1–31.

Manuscript received October 23, 1987
Manuscript accepted May 20, 1988

Appendix 1. Activity relations of the feldspar components in ternary solid solution modified from Ghiorso (1984)

In the following, all X_i's refer to mole fractions of i in the solid.

$$\begin{aligned}
a_{Ab}^{pl(al)} = X_{Ab}\exp\langle\{&W_{Ab,Or}[X_{Or}^2(1 - 2X_{Ab}) \\
&+ X_{Or}X_{An}(0.5 - X_{Ab})] \\
&+ W_{Or,Ab}[2X_{Ab}X_{Or}(1 - X_{Ab}) \\
&+ X_{Or}X_{An}(0.5 - X_{Ab})] \\
&+ W_{Ab,An}[X_{An}^2(1 - 2X_{Ab}) \\
&+ X_{Or}X_{An}(0.5 - X_{Ab})] \\
&+ W_{An,Ab}[2X_{Ab}X_{An}(1 - X_{Ab}) \\
&+ X_{Or}X_{An}(0.5 - X_{Ab})] \\
&+ W_{Or,An}[X_{Or}X_{An}(0.5 - X_{Ab} - 2X_{An})] \\
&+ W_{An,Or}[X_{Or}X_{An}(0.5 - X_{Ab} - 2X_{Or})] \\
&+ W_V P(1 - X_{Ab})X_{Or}\}/RT\rangle.
\end{aligned}$$

$$\begin{aligned}
a_{Or}^{pl(al)} = X_{Or}\exp\langle\{&W_{Ab,Or}[2X_{Ab}X_{Or}(1 - X_{Or}) \\
&+ X_{Ab}X_{An}(0.5 - X_{Or})] \\
&+ W_{Or,Ab}[X_{Ab}^2(1 - 2X_{Or}) \\
&+ X_{Ab}X_{An}(0.5 - X_{Or})] \\
&+ W_{Ab,An}[X_{Ab}X_{An}(0.5 - X_{Or} - 2X_{An})] \\
&+ W_{An,Ab}[X_{Ab}X_{An}(0.5 - X_{Or} - 2X_{Ab})] \\
&+ W_{Or,An}[X_{An}^2(1 - 2X_{Or}) \\
&+ X_{Ab}X_{An}(0.5 - X_{Or})] \\
&+ W_{An,Or}[2X_{Or}X_{An}(1 - X_{Or}) \\
&+ X_{Ab}X_{An}(0.5 - X_{Or})] \\
&+ W_V P X_{Ab}(1 - X_{Or})\}/RT\rangle.
\end{aligned}$$

$$\begin{aligned}
a_{An}^{pl(al)} = X_{An}\exp\langle\{&W_{Ab,Or}[X_{Ab}X_{Or}(0.5 - X_{An} - 2X_{Or})] \\
&+ W_{Or,Ab}[X_{Ab}X_{Or}(0.5 - X_{An} - 2X_{Ab})] \\
&+ W_{Ab,An}[2X_{Ab}X_{An}(1 - X_{An}) \\
&+ X_{Ab}X_{Or}(0.5 - X_{An})] \\
&+ W_{An,Ab}[X_{Ab}^2(1 - 2X_{An}) \\
&+ X_{Ab}X_{Or}(0.5 - X_{An})] \\
&+ W_{Or,An}[2X_{Or}X_{An}(1 - X_{An}) \\
&+ X_{Ab}X_{Or}(0.5 - X_{An})] \\
&+ W_{An,Or}[X_{Or}^2(1 - 2X_{An}) \\
&+ X_{Ab}X_{Or}(0.5 - X_{An})] \\
&- W_V P X_{Ab}X_{Or}\}/RT\rangle.
\end{aligned}$$

Appendix 2. Derivation of a general equation for F_L (fraction of hydrous melt)

For any component i in crystal and melt,

$$\frac{X_i^{s_1}}{X_i^{hm}} = \frac{n_i^{s_1}/(N^0 - N - n_{s_2} - n_{s_3} - \cdots - n_v)}{n_i^{hm}/N}, \quad \text{(A1)}$$

where N^0 and N are the initial number of moles of melt and the current number of moles of melt, respectively; n_{S_2}, n_{S_3}, and n_v represent the number of moles of solid 2, solid 3, and "vapor" (exolved aqueous phase), respectively.

Equation A1 can be rearranged to yield

$$\frac{X_i^{S_1}}{X_i^{hm}} = \frac{n_i^{S_1}}{n_i^{hm}} \cdot \frac{N}{(N^0 - N - n_{S_2} - n_{S_3} - \cdots - n_v)}. \quad \text{(A2)}$$

The following relation can be obtained by multiplying both sides of (2) by N/N^0 (i.e., by the fraction of hydrous melt)

$$\frac{X_i^{S_1}}{X_i^{hm}} = \frac{n_i^{S_1}}{n_i^{hm}} \cdot \frac{F_L}{(1 - F_L - X_{S_2} - X_{S_3} - \cdots - X_v)}. \quad \text{(A3)}$$

Now,

$$n_i^{S_1} = n_i^{hm^0} - n_i^{hm} - n_i^{S_2} - n_i^{S_3} - \cdots - n_i^v \quad \text{(A4)}$$

however, on the basis of the results of Burnham (1967), it will be assumed that $n_i^v \approx 0$. Inserting Equation A4 into A3 yields the following equality

$$(X_i^{S_1}/X_i^{hm})(1 - F_L - X_{S_2} - X_{S_3} - \cdots - X_v) + F_L = (1/X_i^{hm})[X_i^{hm^0} - (n_i^{S_2} + n_i^{S_3} + \cdots)/N^0] \quad \text{(A5)}$$

The ratio $n_i^{S_2}/N^0$ is equivalent to the expression

$$\frac{n_i^{S_2}}{N^0} = \frac{[n_i^{S_2}/(N^0 - N - n_{S_1} - n_{S_3} - \cdots - n_v)]}{[N^0/(N^0 - N - n_{S_1} - n_{S_3} - \cdots - n_v)]} = X_i^{S_2}(1 - F_L - X_{S_1} - X_{S_3} - \cdots - X_v). \quad \text{(A6)}$$

Likewise,

$$n_i^{S_3}/N^0 = (1 - F_L - X_{S_1} - X_{S_2} - X_{S_4} - \cdots - X_v). \quad \text{(A7)}$$

Substituting these expressions into Equation A5 above and solving for F_L yields the equation

$$F_L = [X_i^{hm^0} - X_i^{S_1}(1 - X_{S_2} - X_{S_3} - X_{S_4} - \cdots - X_v) - X_i^{S_2}(1 - X_{S_1} - X_{S_3} - X_{S_4} - \cdots - X_v) - X_i^{S_3}(1 - X_{S_1} - X_{S_2} - X_{S_4} - \cdots - X_v) - \cdots]/(X_i^{hm} - X_i^{S_1} - X_i^{S_2} - X_i^{S_3} - \cdots). \quad \text{(A8)}$$

If several components are used, expressions for X_{S_1} and X_{S_2}, etc., can be derived. In the "granite" system up to three distinct crystalline phases can coprecipitate. The following is a summary of the expressions that can be derived from Equation A8 for this system.

For one solid and melt,

$$F_L = [X_i^{hm^0} - X_i^{S_1}(1 - X_v)]/(X_i^{hm} - X_i^{S_1})$$
$$X_{S_1} = 1 - F_L - X_v.$$

For two solids and melt,

$$F_L = [X_i^{hm^0} - X_i^{S_1}(1 - X_{S_2} - X_v) - X_i^{S_2}(1 - X_{S_1} - X_v)]/(X_i^{hm} - X_i^{S_1} - X_i^{S_2})$$
$$X_{S_2} = \{[X_j^{hm^0} - X_j^{hm}(1 - X_v)](X_i^{S_1} - X_i^{hm}) - [X_i^{hm^0} - X_i^{hm}(1 - X_v)](X_j^{S_1} - X_j^{hm})\}/[(X_i^{hm} - X_i^{S_2})(X_j^{S_1} - X_j^{hm}) - (X_j^{hm} - X_j^{S_2})(X_i^{S_1} - X_i^{hm})]$$
$$X_{S_1} = \frac{[X_i^{hm^0} - X_i^{hm}(1 - X_v) + X_{S_2}(X_i^{hm} - X_i^{S_2})]}{(X_i^{S_1} - X_i^{hm})}.$$

For three solids and melt,

$$F_L = [X_i^{hm^0} - X_i^{S_1}(1 - X_{S_2} - X_{S_3} - X_v) - X_i^{S_2}(1 - X_{S_1} - X_{S_3} - X_v) - X_i^{S_3}(1 - X_{S_1} - X_{S_2} - X_v)]/(X_i^{hm} - X_i^{S_1} - X_i^{S_2} - X_i^{S_3}).$$

$$X_{S_3} = \langle\{[X_k^{hm^0} - X_k^{hm}(1 - X_v)](X_i^{S_1} - X_i^{hm}) - [X_i^{hm^0} - X_i^{hm}(1 - X_v)](X_k^{S_1} - X_k^{hm})\} \cdot [(X_i^{hm} - X_i^{S_2})(X_j^{S_1} - X_j^{hm}) - (X_j^{hm} - X_j^{S_2})(X_i^{S_1} - X_i^{hm})] - \{[X_j^{hm^0} - X_j^{hm}(1 - X_v)](X_i^{S_1} - X_i^{hm}) - [X_i^{hm^0} - X_i^{hm}(1 - X_v)](X_j^{S_1} - X_j^{hm})\} \cdot [(X_i^{hm} - X_i^{S_2})(X_k^{S_1} - X_k^{hm}) - (X_k^{hm} - X_k^{S_2})(X_i^{S_1} - X_i^{hm})]\rangle/\{[(X_j^{hm} - X_j^{S_3})(X_i^{S_1} - X_i^{hm}) - (X_i^{hm} - X_i^{S_3})(X_j^{S_1} - X_j^{hm})] \cdot [(X_i^{hm} - X_i^{S_2})(X_k^{S_1} - X_k^{hm}) - (X_k^{hm} - X_k^{S_2})(X_i^{S_1} - X_i^{hm})] - [(X_k^{hm} - X_k^{S_3})(X_i^{S_1} - X_i^{hm}) - (X_i^{hm} - X_i^{S_3})(X_k^{S_1} - X_k^{hm})] \cdot [(X_i^{hm} - X_i^{S_2})(X_j^{S_1} - X_j^{hm}) - (X_j^{hm} - X_j^{S_2})(X_i^{S_1} - X_i^{hm})]\}.$$

$$X_{S_2} = \{[X_j^{hm^0} - X_j^{hm}(1 - X_v)](X_i^{S_1} - X_i^{hm}) - [X_i^{hm^0} - X_i^{hm}(1 - X_v)](X_j^{S_1} - X_j^{hm}) + X_{S_3}[(X_j^{hm} - X_j^{S_3})(X_i^{S_1} - X_i^{hm}) - (X_i^{hm} - X_i^{S_3})(X_j^{S_1} - X_j^{hm})]\}/[(X_i^{hm} - X_i^{S_2})(X_j^{S_1} - X_j^{hm}) - (X_j^{hm} - X_j^{S_2})(X_i^{S_1} - X_i^{hm})].$$

$$X_{S_1} = [X_i^{hm^0} - X_i^{hm}(1 - X_v) + X_{S_2}(X_i^{hm} - X_i^{S_2}) + X_{S_3}(X_i^{hm} - X_i^{S_3})]/(X_i^{S_1} - X_i^{hm}).$$